Mem. Fac. Eng., Kyoto Univ. Vol. 52, No. 3 (1990)

Turbulence Measurements in Compound Open Channels

by

Akihiro TOMINAGA and Iehisa NEZU†

(Received March 20, 1990)

Abstract

An investigation on a three-dimensional (3-D) turbulent structure including turbulence-driven secondary currents in compound open-channel flows is a very important topic in hydraulic and river engineerings, as well as in fluid mechanics. In this study, accurate measurements in fully-developed compound open-channel flows were conducted by making use of a filder-optic laser Doppler anemometer (FLDA). Secondary velocities could be measured very accurately with the present 3-D measurement system. The characteristics peculiar to compound open channel flows are recognized in a junction region between the main channel and the flood plain, whereas the characteristics in rectangular open channel flows are observed in a region near the side wall of the main channel. Strong inclined secondary currents, which are associated with a pair of longitudinal vortices, are generated in a junction region between the main channel and the flood plain. The primary mean velocity filed is directly influenced by these secondary currents. Turbulence intensisies and the Reynolds stresses are also reveald in detail. Moreover, the effects of channel gemetry and bed roughness on turbulent structures are examined.

1. Introduction

The turbulent structures in compound open channels are characterized by high shear layers which are generated by the difference of velocity between the main-channel flow and the flood-plain flow. In these high shear-layer regions, there exist not only vortices with, vertical axes, but also vortices with longitudinal axes. The latter is the so-called "secondary currents" in the cross section of channels, which are driven by anisotropy of turbulence. The secondary currents are found to influence the primary mean-velocity field in the same mechanism as in square and rectangular channels [e.g. see an excellent review conducted by Bradshaw (1987)]. It is necessary to experimentally reveal the

Department of Civil Engineering, Gunma University, Kiryu 376, Japan.
† Department of Civil Engineering, Kyoto University, Kyoto 606, Japan.

turbulent structures as well as the seconadry currents in compound open channel flows. It is then necessary to develop the three-dimensional (3-D) calculation techniques with refined turbulence modelling in order to predict turbulent structures, friction laws and sediment transport in compound rivers.

Many experimental researches have been carried out to clarify the distributions of the mean velocity and boundary shear stress in compound channel flows, using the conventional Pitot static tube and the Preston tube [e.g. Myers & Elsawy (1975), Rajaratnam & Ahmadi (1981), Knight & Demetriou (1983), Knight & Hamed (1984) and Nalluri & Judy (1985)]. However, only a few measurements of turbulence characteristics have been recently conducted in compound open channel flows by making use of hot-film anemometers [e.g. Prinos et al. (1985)] and of the one-component Laser Doppler anemometer (LDA) [e.g. Mckee et al. (1985)]. On the other hand, two-dimensional (2-D) turbulence modellings of compound open-channel flows were developed to give the depth-averaged flow characteristics [e.g. Pasche et al. (1985), Alavian & Chu (1985), Ogink (1985) and Keller & Rodi (1988)]. Very recently, three-dimensional (3-D) numerical calculation techniques have been also developed to reproduce turbulent structures in compound open-channel flows [e.g. Krishnappan & Lau (1986), Kawahara & Tamai (1988), Larsson (1988) and Prinos (1989)]. However, the structure of the secondary currents in compound open-channels are not yet available at present. The detailed experimental data of the three-dimensional (3-D) turbulent structure and the associated secondary currents are necessary to improve 2-D and 3-D calculation techniques for predicting the three-dimensional velocity distributions, bed shear stress distributions and the associated heat and mass transport in compound open-channel flows.

It is very difficult to accurately measure the secondary velocity components in open channel flows, because they are only 1 to 3% of the primary mean velocity. In a square-duct air flow, Brundrett & Baines (1964) measured all three components of the mean velocity and all six components of the Reynolds stress, by making use of hot wire anemometers. On the other hand, Melling & Whitelaw (1976) could first measure five components of the Reynolds stress and all three components of the mean velocity, using one component laser Doppler anemometer (LDA). A LDA system is considered to the most accurate instrument of velocity measurements, particularly for the measurenents of secondary velocities, because the laser beams of LDA never disturb fluid flows and furthermore no calibration of LDA is needed. As to open-channel flows, Nezu & Rodi (1985) first carried out some accurate measurements of secondary currents in rectangular open-channel flows, by making use of two-component LDA system.

They found that the secondary current patterns in open channel flows were quite different from those of closed channel flows; this difference was caused by the existence of the free surface. However, the LDA measurements by Nezu & Rodi (1985) were restricted to two components of the mean-volocity and three components of the Reynolds stress. The production term of turbulence-driven secondary currents, i.e. the difference of the normal stress gradients, could not, therecore, be examined in Nezu & Rodi (1985). Tominaga & Ezaki (1988) and Tominaga et al. (1989) have recently conducted some measurements of the primary mean velocity and secondary currents in open-channel flows with various cross sections, using X-type hot-film anemometers. These results revealed the characteristics of turbulent flows in rectangular, trapezoidal and compound open channels. Very recently, Arnold et al. (1989) and Tominaga et al. (1989) have conducted some measurements of turbulent structures in compound open channel flows by making use of the two-component Laser Doppler anemometer (LDA). Accurate experimental data of turbulence in open-channel flows are required not only to understand a comprehensive mechanism of 3-D turbulent structures, but also to develop mathematical turbulence models including the effects of the free surface.

In the present study, more accurate measurements were conducted using a fiber-optic Laser Doppler anemometer (FLDA). The three-dimensional distribution of the mean velocity and the associated turbulent characteristics were revealed from the FLDA database. The effect of the ratio of the flood plain depth to the main channel depth on the secondary currents and turbulent structure were investigated, involving the roughness effects in the flood plain on these features. The bed shear stress distributions in the main channel and flood plain flows were evaluated from the log-law distribution. Finally, the interaction of the main-channel and flood plain flows was discussed using the momentum equation.

2. Experimental Equipments and Measurement Techniques

2. 1 open-channel flume and experimental condition

The experiments were conducted in a tilting flume with 12.5 m length and 40 cmx 40 cm cross section. The bed-was composed of a painted iron plate and the side-walls were composed of glass. Water was pumped from a ground pool to a constant-head tank from which the water flowed by gravity into a flume through a settling chamber, as shown in Fig. 1. Mesh screens and a honeycomb were set up in the settling chamber at the entrance of the channel in order to

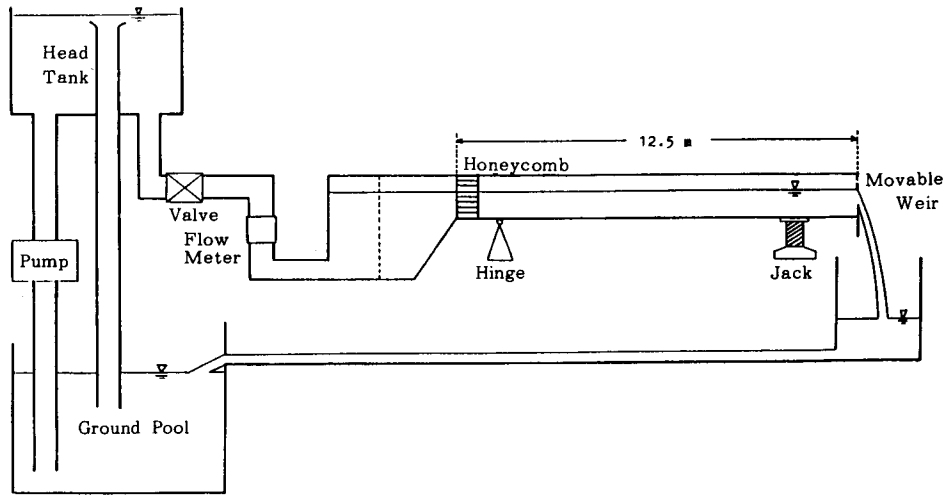

Fig. 1 Experimental Open-Channel Flume

prevent large disturbances and to establish a fullydeveloped and uniform flow at the test section 7.5 m downstream from the entrance of the channel. Unsymmetrical compound open channels were composed of a main channel and a flood plain made of vinyl-chloride plate on one side in the flume. The nomenclature used in this paper is also indicated in Fig. 2. B is the total channel width, b is the main-channel width, H is the flow depth of the main channel and D is the height of flood plain.

Experimental conditions are shown in Table 1. $\overline{U}_*$ is the friction velocity averaged along the bed, which was evaluated from the log-law distributions. Four experiments, i.e. Case S-1, S-2, S-3 and R-1, were conducted in this study. The cases S-1, S-2 and S-3 had smooth boundaries on the entire perimeter, and the height D of the flood plain was changed from 2 cm, 4 cm to 6

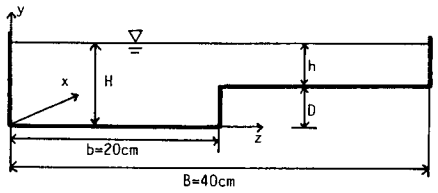

Fig. 2 Schematic Description of Flood Plain Open Channel Flow

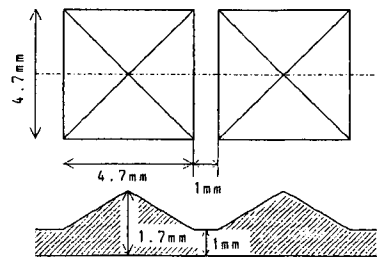

Fig. 3 Roughness Element

Table 1 Experimental Conditions

CASE	Flow depth of main channel H (cm)	Flow depth of flood plain h (cm)	Maximum velocity U_{max} (cm/s)	Friction velocity $\overline{U}_*$ (cm/s)	Mean bulk velocity U_m (cm/s)	Reynolds number $Re \equiv (4U_mR/\nu)$	Froude number $Fr \equiv (U_m/\sqrt{gh})$
S−1	8.03	6.03	40.9	1.64	36.8	6.72×10^4	0.415
S−2	8.00	4.00	38.9	1.64	34.9	5.45×10^4	0.393
S−3	8.05	2.05	35.8	1.41	28.8	4.56×10^4	0.402
R−1	8.05	4.05	35.2	1.61	27.7	3.97×10^4	0.312

R is the hydraulic radius and ν is the kinematic viscosity.

cm, respectively. On the other hand, case R-1 had a rough bed on the bottom of the flood plain. The commercially available antiskid mat shown in Fig. 3 was used as the rough bed in the case of R-1. The equivalent sand roughness k_s of this rough bed was equal to 0.2 cm. The average value of $k_s^+ \equiv U_* k_s/\nu$ was then equal to 34, which lies in the range of incomplete roughness, i.e. $5 \leqq k_s^+ \leqq 70$. Experimental conditions are shown in Table 1. The distance x= 7.5 m from the channel entrance to the test section corresponds to x/4R= 37.4, 43.8, 52.1 and 43.8 in the cases of S-1, S-2, S-3, and R-1, respectively, where R is the hydraulic radius. U, V and W denote the components of the mean velocity; u, v and w the velocity fluctuations; and u′, v′ and w′ the turbulence intensities in the x-axis (streamwise direction), y-axis (vertical direction) and z-axis (spanwise direction), respectively.

2. 2 FLDA optical system

The velocity measurements were carried out using a two-color fiber-optic laser Doppler anemometer (FLDA) that is made by the KANOMAX-TSI company. This FLDA system was operated in the backward-scattering differential mode. A 2 W high-power Argon-ion laser was used to improve the burst signals from the FLDA. Four beams of blue (wave length λ= 488 nm) and green (λ= 514.5 nm) lights were frequency-shifted (500 KHz) by double Bragg cell modules and then transmitted into the optical probe through optical transmitting fibers. The optical probe was composed of 45 mm in diameter and 200 mm in length. The four beams were focused onto the measuring point by a front lens with a 250 mm focal length. The half angle ϕ of the beam intersection was 3.3° (see Fig. 4).

The optical probe was set up beside the side wall of the main channel, when the streamwise (x-axis) and vertical (y-axis) velocity components (u, v) were measured. On the other hand, the optical probe was set up above the free

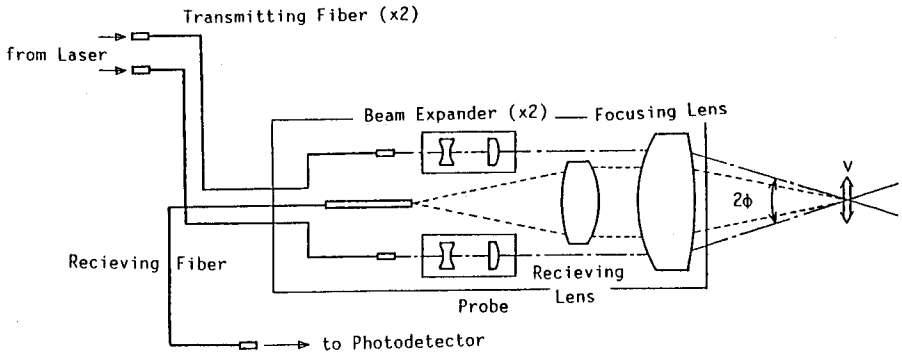

Fig. 4 FLDA Probe System

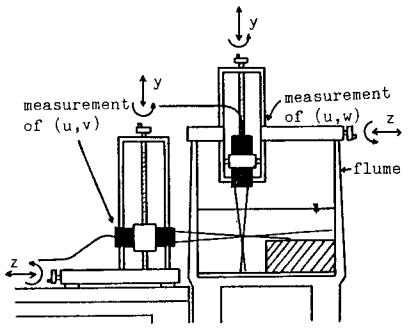

Fig. 5 Measuring System using FLDA

surface, when the streamwise and spanwise (z-axis) velocity components (u, w) were measured, as shown in Fig. 5. The movement of the traversing mechanism for the optical probe could be controlled with an accuracy of 0.1 mm, as shown in Fig. 5. The measurements of (u, v) were conducted in the region of $z \leqq 30$ cm because of the limitation of the focal length of the optical probe in water. The two-color FLDA system could not be operated in the regions where the beams were intercepted by the channel bed and by the free surface. Only the streamwise velocity component U in this region was then measured by the usual two -beam method. Since the undulation of the free surface was sufficiently small, the present FLDA system operated above the free surface was feasible for the velocity measurements of (u, w) with reasonable accuracy. This validity was checked by comparing the distributions of the streamwise mean velocity U and the turbulence intensity u' obtained from the (u, w) -measurements with those obtained from the (u, v) -measurements. The error between the measured values of U was within about $\pm$ 1.5% of the maximum velocity U_{max} and the error of

the measured values of u' was within $\pm$ 3% of the maximum turbulence intensity u'_{max}. Furthermore, the spectra of u in both measurements coincided well with each other. As a result, it was concluded that the (u, w) measurements could be made accurately in the present study.

2. 3 Data-processing method

The Doppler signals were processed with frequency trackrs (KANOMAX 8015 B). The condition of the present experiments, in which the turbulence intensities were moderate and a concentration of scattering particles was comparatively high, was satisfactory for a frequency tracker. The output signgfs from the frequency trackers were digitized using an A-D converter with sampling frequency 100 Hz and sampling time 50 seconds.

The angle θ of each pair of beams against the streamwise axis was set as $\theta = 45°$ by eye, in order to give a sufficient number of Doppler bursts for accurate processing. A small deviation of the angle $\Delta\theta$ from this chosen valus must be corrected for accurate measurements of the secondary velocity. The velocity components u and v in the x- and y-directions, respectively, were evaluated from the following theoretical relations including this deviation angle $\Delta\theta$ [e. g. Nezu & Rodi (1986)];

$$\tilde{u}=\frac{1}{\sin 2\theta}[\tilde{u}_2\sin(\theta-\Delta\theta)+\tilde{u}_1\sin(\theta+\Delta\theta)] \tag{1}$$

$$\tilde{v}=\frac{1}{\sin 2\theta}[\tilde{u}_2\cos(\theta-\Delta\theta)-\tilde{u}_1\cos(\theta+\Delta\theta)] \tag{2}$$

$$\tilde{u}_1=\frac{\lambda_1}{2\sin\phi}(f_1-f_{s1}),\quad \tilde{u}_2=\frac{\lambda_2}{2\sin\phi}(f_2-f_{s2}) \tag{3}$$

in which $\tilde{u}_i$ for $i=1$ (green beam) and 2 (blue beam) are the velocity components measured directly by the green and blue beams. f is the Doppler frequency and f_s is the shift frequency. By setting $\theta=45°$, the mean velocities U, V and the Reynolds stresses u'^2, v'^2 and $-\overline{uv}$ are obtained from Eqs. (1) and (2);

$$U=U_M\cos\Delta\theta-V_M\sin\Delta\theta,\quad V=V_M\cos\Delta\theta+U_M\sin\Delta\theta \tag{4}$$

$$u'^2=u'^2_M\cos\Delta\theta-2\overline{u_Mv_M}\sin\Delta\theta,\quad v'^2=v'^2_M\cos\Delta\theta+2\overline{u_Mv_M}\sin\Delta\theta \tag{5}$$

$$\overline{uv}=\overline{u_Mv_M}\cos\Delta\theta+(u'^2_M-v'^2_M)\sin\Delta\theta \tag{6}$$

in which suffix M denotes the measured value. $\Delta\theta_1$ arising from a small misalignment of the beams against the streamwise axis in the (u, v) -measurements can be evaluated as follows;

$$\tan\Delta\theta_1=-\frac{1}{bD}\int_0^D\int_0^b\left(\frac{V_M}{U_M}\right)dz\ dy \tag{7}$$

in which b is the main channel width and D is the height of the flood plain. Because the velocity could not be measured over the entire channel width, a mass conservation should be cosidered in the main channel region $y\leqq D$. As to the (u, w) -measurements, the velocity components were obtained in the same manner as the (u, v) -measurements, in which the V-component was replaced by the W-component in Eqs. (2), (4), (5) and (6). $\Delta\theta_2$ in the (u, w) -measurements can be estimated, as follows;

$$\tan\Delta\theta_2=-\frac{1}{bH}\int_0^b\int_0^H\left(\frac{W_M}{U_M}\right)dz\ dy \tag{8}$$

In the present experiments, $\Delta\theta_1$ and $\Delta\theta_2$ were within only 0.5°.

3. Experimental Results and Discussions

In the present experiments, the strongest secondary currents appeared in the case of S-2 ($h/H=0.5$), and thus this experimental case is considered to be a typical one which describes the characteristics of compound openchannel flows, as pointed out by Tominaga et al. (1989). Therecore, the basic structure of all three components (U, V, W) of the mean velocity, all three components (u', v', w') of the turbulence intensity and two components ($-\overline{uv}$, $-\overline{uw}$) of Reynolds stress are discussed in detail for the case of S-2.

3. 1 Secondary Currents (Longitudinal Vortex)

Fig. 6(a) shows the vector description of the secondary currents (V, W) normalized by the maximum mainstream velocity U_{max}. The magnitude of velocity is shown as a unit arrow at the top-side of this figure. The values of V and W in a fully-developed turbulent flow must satisfy the equation of continuity, as follows;

$$\frac{\partial V}{\partial y}+\frac{\partial W}{\partial z}=0 \tag{9}$$

A degree of accuracy of the present measurements should be discussed by checking whether the experimental values of V and W satisfy the equation of continuity, Eq.(9). The stream function ϕ of the secondary currents is defined by setting $\phi=0$ at $y=H$, as follows;

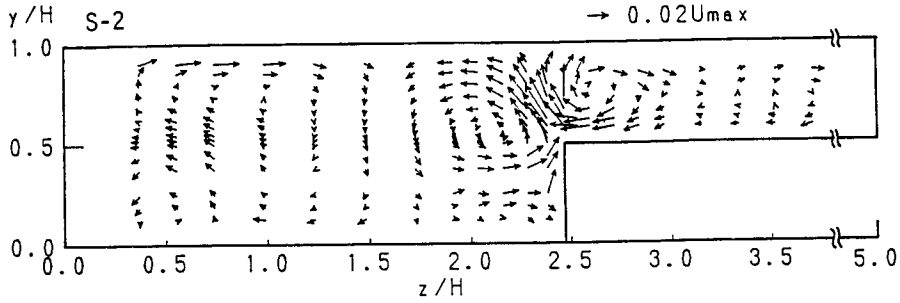

(a) Measured Secondary Current Vectors

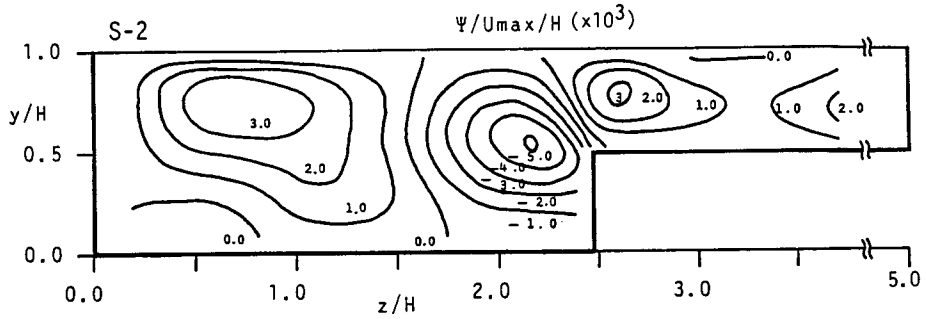

(b) Calculated Stream Function ϕ

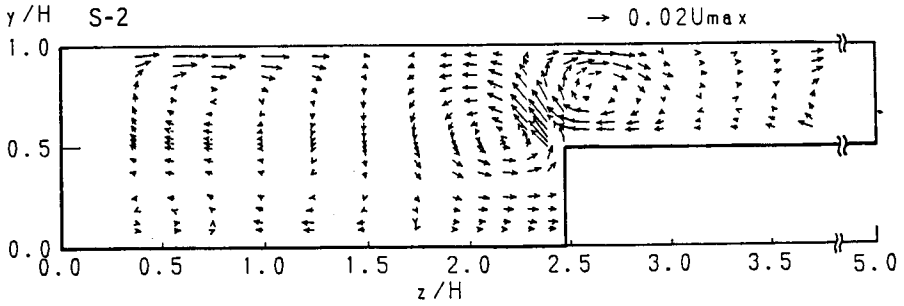

(c) Calculated Secondary Current Vectors

Fig. 6 Structure of Secondary Currents

$$\phi = -\int_y^H W dy \tag{10}$$

The isolines of the calculated stream function ϕ, which indicate the stream lines of the secondary currents, are shown in Fig. 6 (b). The secondary velocity components V and W are, of course, obtained by differentiating these calculated curves

of ϕ. Fig. 6(c) shows the vector description of such calculated values of V and W. The measured secondary currents of the cross section coincide well with the calculated values from the stream function ϕ which was obtained from Eq.(10). This implies that the measured values of the secondary velocity reasonably satisfy the equation of continuity. Consequently, it is concluded that the present FLDA measurements are very accurate.

Strong inclined secondary currents are generated from the junction edge toward the free surface in compound open-channel flows, as clearly seen in Fig. 6. The magnitude V_s of the secondary currents and its direction angle θ_s against the z axis are defined as follows;

$$V_s=(V^2+W^2)^{1/2} \tag{11}$$

$$\theta_s=\tan^{-1}(V/W) \tag{12}$$

The maximum magnitude of V_s is about 4% of U_{max}. This value is slightly greater than the maximum magnitude of the secondary currents observed near the free surface in narrow rectangular open channels, as has been indicated by Nezu & Rodi (1985), Tominaga et al. (1989) and Nezu et al. (1989); the latter is 2 - 3% of U_{max}. It is generally said that the order of the maximum magnitude of the turbulence-driven secondary currents is as large as a few percent of the primary mean velocity. The direction angle θ_s is about 60° in a compound open-channel flow.

A pair of secondary currents are recognized on both sides of the inclined upflow. These currents can be regarded as "longitudinal vortices". The vortex on the side of the flood plain is called here the "flood-plain vortex", whereas the vortex on the side of the main channel is called the "main-channel vortex". Both of these vortices reach the free surface and cover the junction region of $1.6 \leqq z/H \leqq 3.0$ in the spanwise direction.

In the side-wall region of the main channel ($z/H \leqq 1.5$), a horizontal flow from the side wall to the centre of the main channel appears clearly at the free surface, and its flow forms the longitudinal vortex, the so-called "free-surface vortex". This free-surface vortex is generated due to the anisotropy of turbulence which is caused by the existence of the free surface and side wall. The same mechanism is also seen in the rectangular openchannel flows, which have been recently verified by Nezu & Rodi (1985), Tominaga et al. (1989) and Nezu et al. (1989). All of them found that the spanwise scale of the free-surface vortex in rectangular open-channels reaches about $2H$, when the aspect ratio B/H is greater than 5. Therefore, the free-surface vortex meets the main-channel vortex at the central region of the main channel, i.e., at about $z/H=1.6$. The

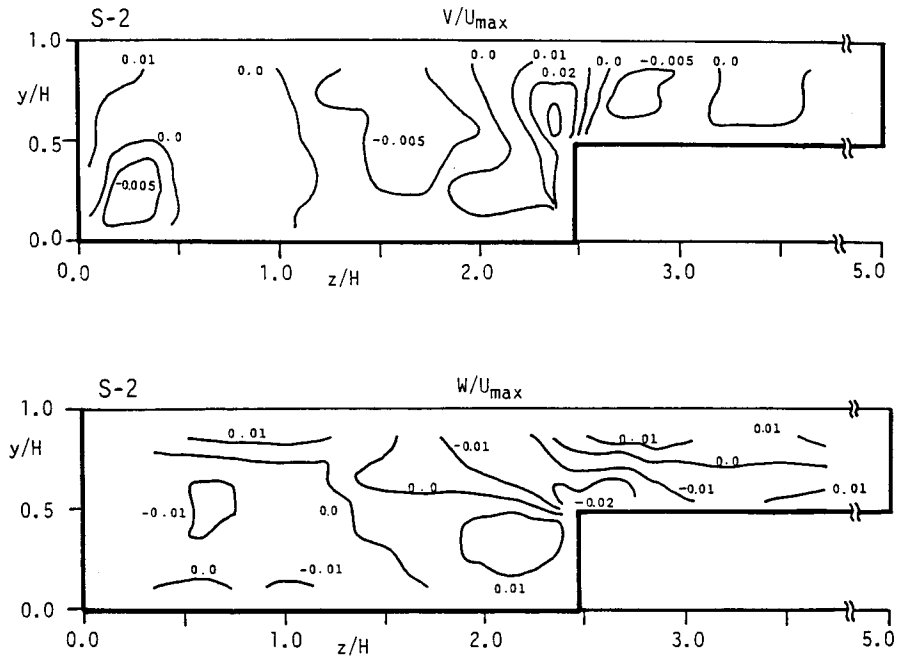

Fig. 7 Isolines of Secondary Current Velocity

bottom vortex, which exists in the corner of rectangular channels, can be also recognized in the region $z/H \leqq 0.8$.

Fig. 7 shows isolines of the secondary velocities V and W normalized by U_{max}. The vertical mean velocity V attains a large positive value near the junction edge and has a comparatively sharp peak. On both sides of this positive region, V indicates a relatively small negative value. On the other hand, the spanwise velocity W indicates a negative value along the inclined line from the junction edge and indicates positive values below and above this region. The absolute values of negative and positive regions are almost the same order of magnitude.

3. 2 Distributions of Primary Mean Velocity

Fig. 8 shows the isovel lines of the primary mean velocity $U(y, z)$ normalized by U_{max}. Isovel lines bulge significantly upward in the vicinity of the junction edge along the inclined upflow shown in Fig. 6. The same phenomena were also observed by Lai & Knight(1988) in the wind tunnel experiments. The velocity in this region is decelerated due to low-momentum transport by the

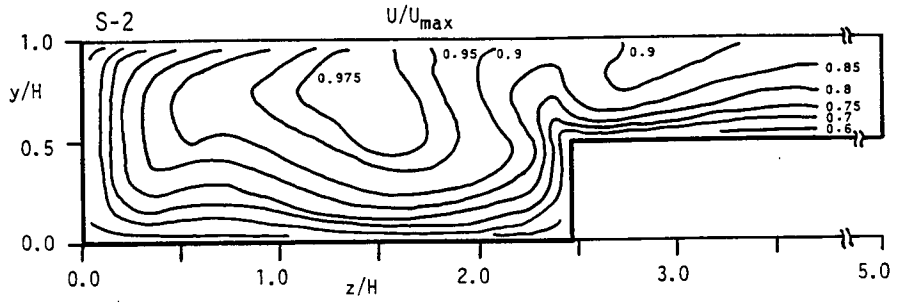

Fig. 8 Isovels of Primary Mean Velocity U

secondary currents away from the wall. On both sides of this decelerated region, the isovel lines bulge toward the walls, i.e. the bed of the flood plain and the side wall at the junction, due to the high-momentum transport by the secondary currents.

In the side wall region ($z/H \leqq 1.5$), the deceleration near the free surface can be clearly seen, and these isovel lines bulge toward the side wall in the same manner as the rectangular open channels. The deceleration due to the bottom vortex is also recognized near the bed at about $z/H = 0.75$. Of particular significance is that the maximum velocity tends to appear below the free surface even in the central region of the main channel. On the other hand, the velocity near the bed is accelerated due to the high momentum transport of the down-flow. Nezu & Rodi(1985) and Tominaga et al. (1989) pointed out that the velocity-dip phenomenon is peculiar to narrow open-channels, the aspect ratio B/H of which is smaller than 5. It is expected that the 3-D turbulent structure of the main channel approaches that of the narrow rectangular open-channel, as the flood-plain region decreases. Consequently, the structure of the primary mean velocity is directly affected by the momentum transport due to the secondary currents.

Fig. 9 shows the distribution of $U^+ \equiv U/U_*$ against $y^+ \equiv yU_*/\nu$ at each span-wise position in the main-channel region near the junction and in the flood-plain region. The broken line in this figure indicates the log-law distribution;

$$\frac{U}{U_*} = \frac{1}{\kappa} \ln\left(\frac{yU_*}{\nu}\right) + A \tag{13}$$

in which $\kappa = 0.41$ and $A = 5.3$ were abopted here according to the results of Nezu & Rodi(1986) for open channels.

The primary mean velocity in the range of $y^+ < 400$ for the main channel

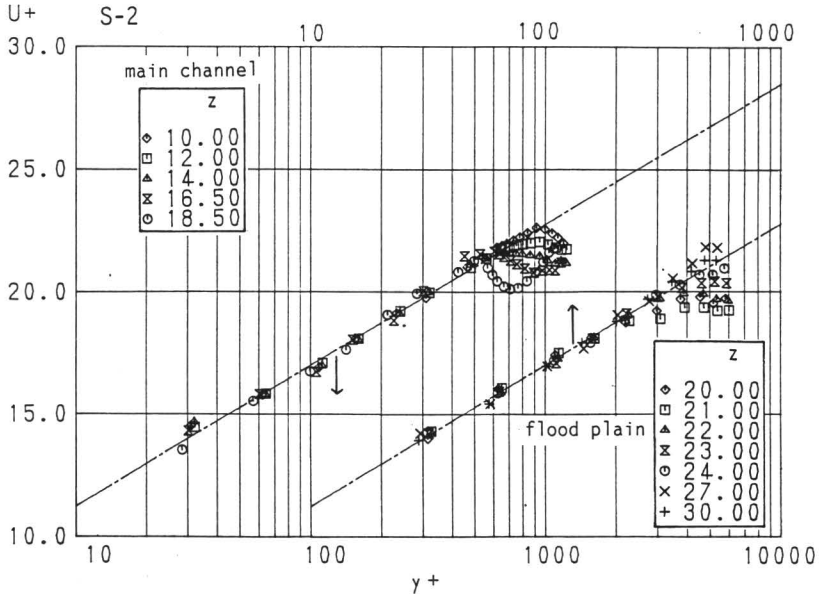

Fig. 9 Log-Law Distributions of Primary Mean Velocity

and also in the range of $y^+ < 200$ for the flood plain coincided well with the log-law distribution, except for very near the side wall.

The distributions of U in the outer region, i. e. free-surface region, deviate from the log-law due to the low-momentum transport in the spanwise direction. The magnitude of the defect of the velocity from the log-law distribution becomes greater as the junction is approached. At the position $z = 18.5$ cm, the distribution of U begins to decrease at the heght $y=D$ and again increases rapidly after attaining a minimum value.

3. 3 Distribution of Reynolds Shear Stresses

Fig. 10 shows the isolines of Reynolds stresses $-\overline{uv}$ and $-\overline{uw}$ normalized by the averaged friction velocity $\overline{U}_*^2$. The Reynolds shear stresses are generally related to gradients of the primary mean velocity. The negative value of $-\overline{uv}$ appears in a region below the outline of the inclined upflow and also in a free-surface region of $z/H < 1.3$. The former region is one of the most essential characteristics in compound open channels. On the other hand, the latter region is peculiar to rectangular open channels, as pointed out by Nezu & Rodi(1985) and Nezu et al. (1989). The negative region of $-\overline{uv}$ corresponds well to the region where $\partial U/\partial y$ is negative. In the flood plain, the value of $-\overline{uv}$ increases just above the junction edge adjacent to the negative region, and it decreases to

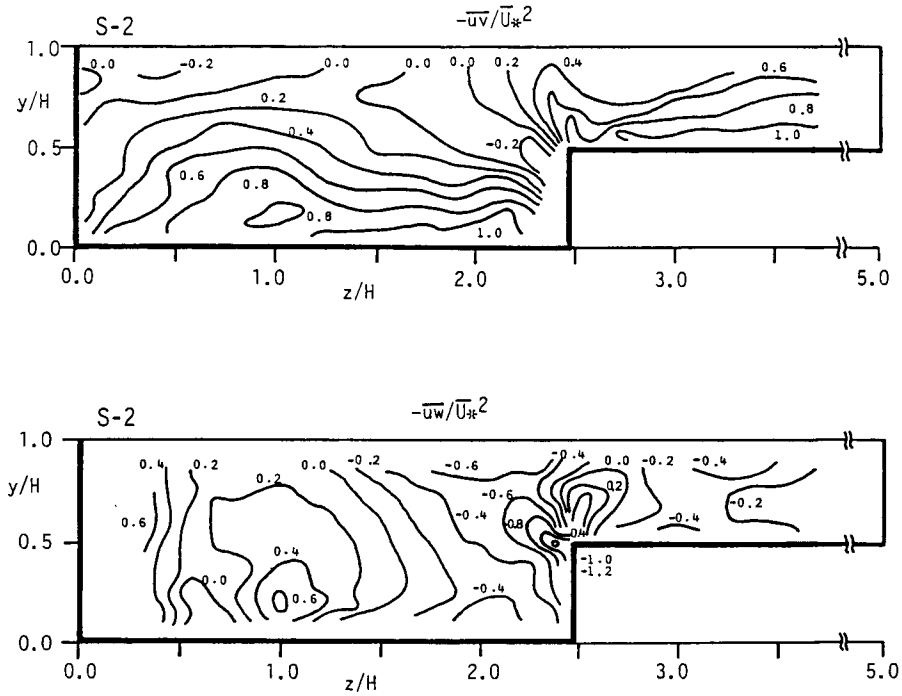

Fig. 10 Isolines of Reynolds Stresses $-\overline{uv}$ and $-\overline{uw}$

be minimum at a position slighty away from the junction edge. Observing the positive isolines of $-\overline{uv}$ in the main-channel, the isolines are inflected markedly at about $z/H=1.5$, and the value in a region $z/H>1.5$ becomes small except very near the bed. Comparing this isoline with the isoline of U, it is concluded that turbulence becomes small in the region where U is accelerated by the downflow, whereas it becomes large in the region where U is decelerated by the upflow.

The value of $-\overline{uw}$ becomes zero at about $z/H=1.5$, and the sign of $-\overline{uw}$ is positive in the side of the main-channel side wall, whereas it is negative in the opposite side. The nagative value of $-\overline{uw}$ appears near the bed at about $z/H=0.6$, which indicates an existence of a bottom vortex. Of particular significance is that the value of $-\overline{uw}$ in the vicinity of the junction attains a negative peak on the side of the main channel, whereas it attains a positive peak on the side wall of the flood plain. This implies that there exists momentum transport from the main channel toward the flood plain. The same mechanism has also been pointed out in duct flow by Gessner(1973). The sign of $-\overline{uw}$ also corresponds to

that of $\partial U/\partial z$. This fact suggests that the eddy viscosity model is valid even in this complex flow, but the spatial distribution of eddy viscosities in the cross section is very complicated.

3. 4 Turbulent Kinetic Energy and Turbulence Intensities

Fig. 11 shows the isolines of the turbulent kinetic energy $k \equiv (u'^2+v'^2+w'^2)/2$, which are normalized by the averaged friction velocity $\overline{U}_*$. The isolines of k bulge in the inclined outward direction from the junction edge in the same manner as the primary mean velocity shown in Fig. 8. This implies that the total magnitude of turbulence increases in the vicinity of the junction edge. However, the bulge of k–isolines is not so strong as that of the U–isolines along the inclined upflow. The isolines of k below the flood–plain elevation are inflected at the centre of the main channel, in the same manner as those of the Reynolds stress $-\overline{uv}$.

Fig. 12 shows the isolines of all three conponents of the turbulence intensities u', v' and w', which are normalized by the averaged friction velocity $\overline{U_*}$. All three components of the turbulence intensity increase in the vicinity of the junction edge. Carefully observing the isolines near the junction edge, it should be noted that the behavior or the isolines of u', v' and w' are different from eack other. The isolines of u' seem to bulge from the junction edge in both the vertical and spanwise direction, but they seem to cave in the direction of the inclined upflow, as contrasted with the isolines of the primary mean velocity shown in Fig. 8. On the other hand, the isolines of v' tend to bulge in the vertical direction in the main–channel region beside the junction, whereas the isolines of w' tend to bulge in the spanwise direction near the junction edge. This implies that the effect of convection due to the secondary currents on turbulence intensities is much more complicated than those of the primary–mean

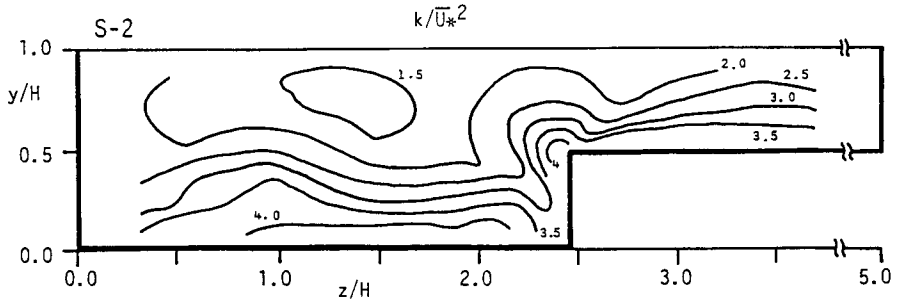

Fig. 11 Isolines of Turbulent Kinetic Energy k

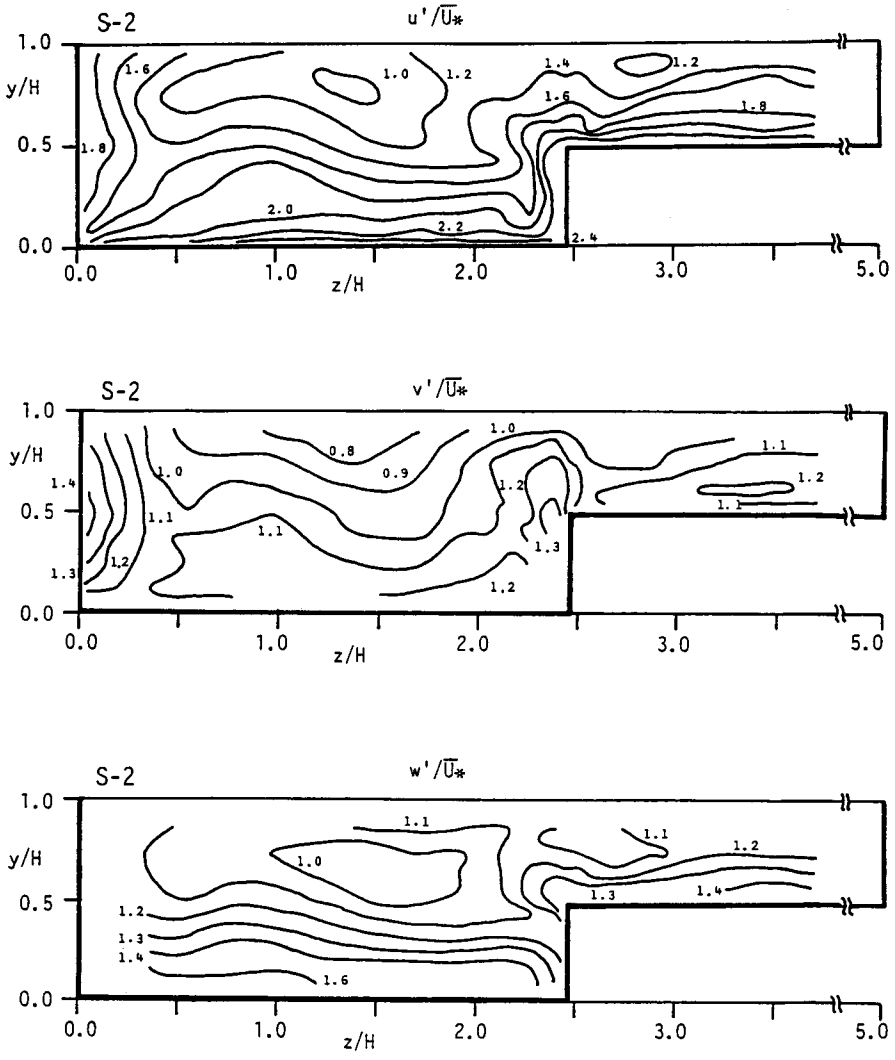

Fig. 12 Isolines of Turbulence Intensities u', v' and w'

energy and the turbulent kinetic energy. Consequently, the pattern of v' near the junction is quite different from that of w'. This means that the turbulence near the junction indicates a strong anisotropic behaviour. Such significant differences in the distributions of u', v' and w' represent an anisotropic redistribution of the turbulence energy into three components from the mean flow energy. It is therefore necessary to explain reasonably the redistribution of the

turbulence energy, using a refined turbulence modelling such as algebraic stress models and full stress models.

It should be noted that the minimum value of u' appears not on the free surface, but below it in the main channel. This feature corresponds well to the velocity-dip phenomenon, which was also observed in narrow rectangular channels by Nezu et al. (1989). The same feature as u' is recognized in the distribution of w'. The degree of increase of w' at the free surface seems to be greater than u'. On the other hand, the value of v' decreases monotonically as the free surface is approached. These facts are essential to open channel flows, and such an anisotropy of the turbulence generates the secondary currents peculiar to open channel flows, as indicated by Tominaga et al. (1989).

Fig. 13 shows the productions of turbulent kinetic energy, $P_1=-\overline{uv}\partial U/\partial y$, $P_2=-\overline{uw}\partial U/\partial z$ and $P=P_1+P_2$, respectively. The magnitude of these terms was by one order greater the convection terms $V\partial k/\partial y$ and $W\partial k/\partial z$ in the turbulent energy equation. A noticeable relationship is recognized between the turbulence intensities and the productions. The regions with large values of v' correspond to the regions with large values of P_2. The isolines of w' are similar to those of P_1, whereas the isolines of u' are similar to those of the total production P. These facts suggest that the 3-D structures of turbulence intensities are strongly correlated with the production of turbulent kinetic energy. This relationship described here gives important information about turbulence modelling.

Fig. 14 (a) shows the isolines of the difference $(\overline{w^2}-\overline{v^2})$ of the normal stresses. They represent the anisotropy of turbulence and thus determine the structure of the secondary currents driven by the turbulence. The value of $(\overline{w^2}-\overline{v^2})$ decreases with y/H and attains a minimum at $y/H=0.6-0.7$. Then, it increases again toward the free surface.

This anisotropy of turbulence generates the free-surface vortex and bottom vortex, as verified by Tominaga et al. (1989) and Nezu et al. (1989). Of particular significance is that the values of $(\overline{w^2}-\overline{v^2})$ near the junction become negative and indicate complicated behaviors. Fig. 14 (b) shows the isolines of the production term $\partial^2(\overline{w^2}-\overline{v^2})/\partial y\partial z$ of secondary currents in the streamwise equation of vorticity. The absolute value of $\partial^2(\overline{w^2}-\overline{v^2})/\partial y\partial z$ becomes very large closer to the junction edge, and attains positive and negative peaks alternately in this region. Consequently, this gradient becomes a driving force to generate an inclined upflow in the same mechanism as the corner secondary flow. However, this production mechanism of the secondary currents is too complicated to verify the generation mechanism using experimental data, as has been discussed by Tominaga et al. (1989). In order to accurately predict the secondary currents in

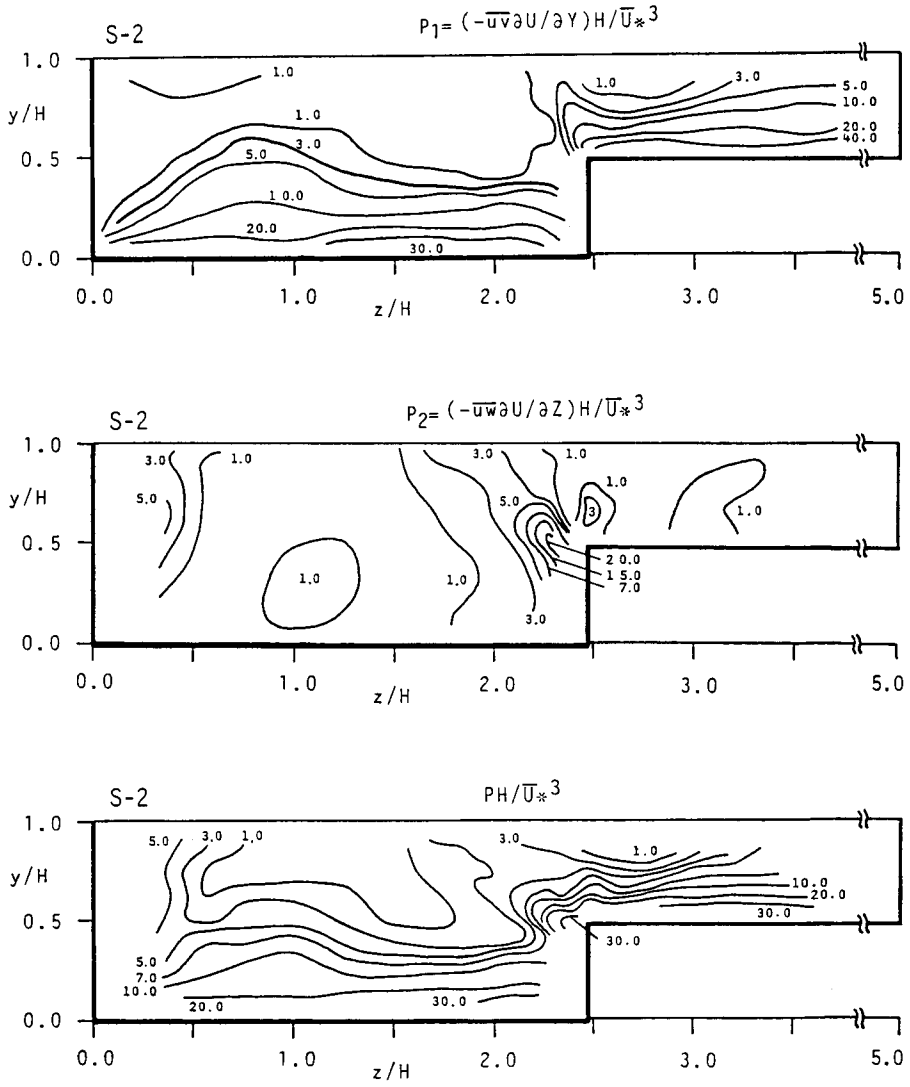

Fig. 13 Isolines of Productions of Turbulent Kinetic Energy

compound open-channel flows, refined computational techniques are necessary, elaborately involving significant anisotropy of turbulence.

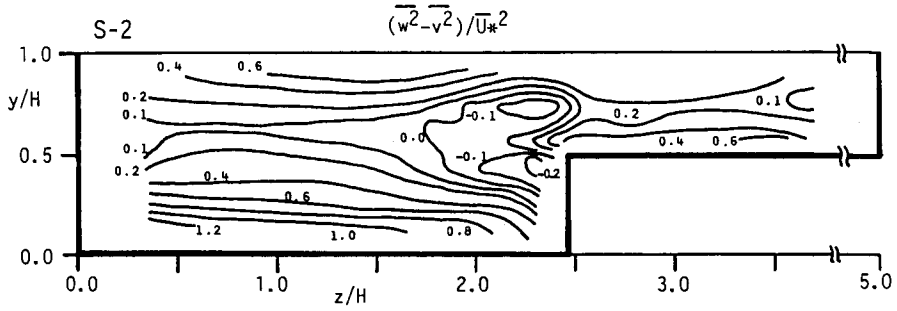

(a) Isolines of $(\overline{w^2}-\overline{v^2})$

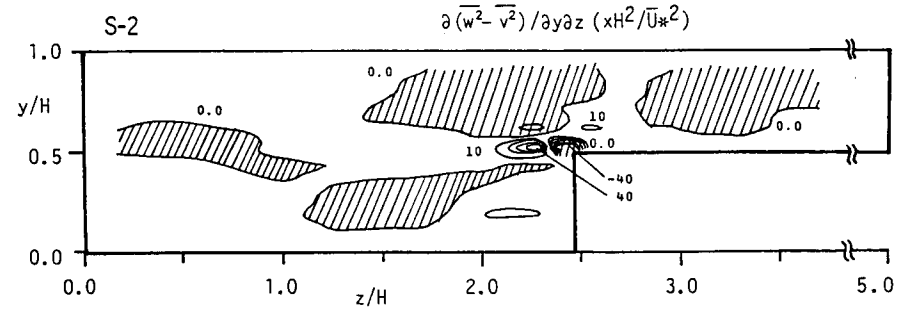

(b) Isolines of $\partial^2(\overline{w^2}-\overline{v^2})/\partial y\partial z$

Fig. 14 Anisotropy of Turbulence

4. Effects of Channel Geometry and Wall Roughness

4. 1 Secondary Currents

Fig. 15 (a) and (b) show the vector descriptions of the secondary currents for the cases of S-1 ($h/H=0.75$) and S-3 ($h/H=0.25$). Because the spanwise velocity component W in the region closer than 1.0 cm to the wall and the vertical velocity component V in the region closer than 1.1 cm to the free surface could not be measured with the present FLDA system, no experimental data of (V, W) were available over the flood plain in the case of S-3. The inclined upflow is also generated in the cases of S-1 and S-3. The maximum magnitude of the inclined upflow becomens about 3.5% and 2.5% of U_{max} respectively. In the case of S-1, the main-channel vortex is not recognized clearly, while the

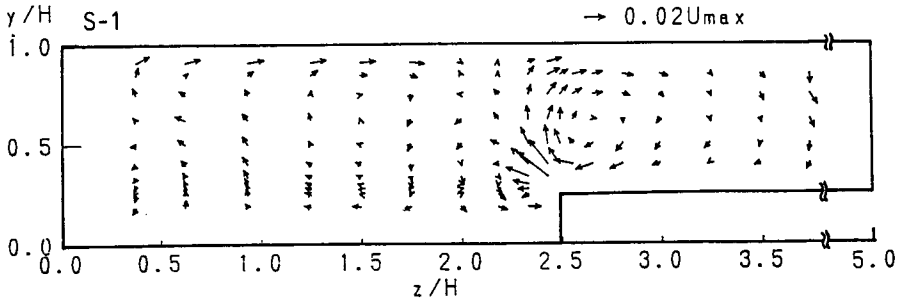

(a) Case S-1 (h/H=0.75)

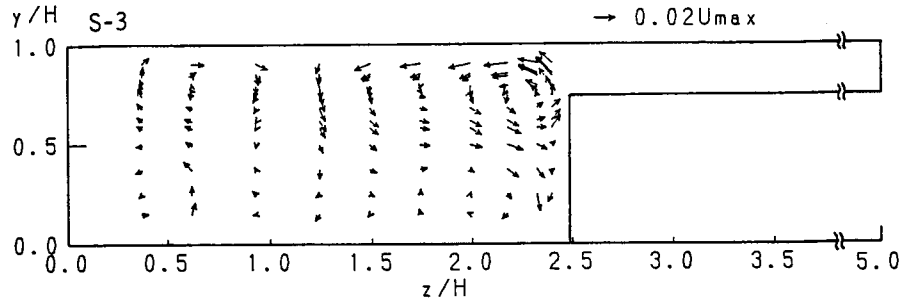

(b) Case S-3 (h/H=0.25)

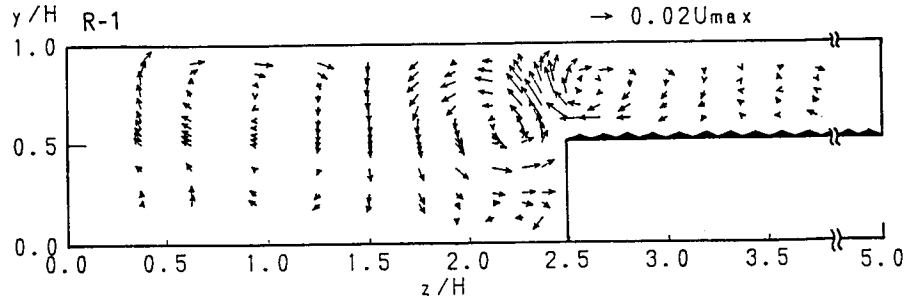

(c) Case R-1 (h/H=0.5 and rough on the flood plain)

Fig. 15 Secondary Current Vectors in Various Cases

flood-plain vortex is strong enough to reach the free surface. The direction of the inclined upflow becomes almost vertical at the middle of the flow depth. The free-surface vortex prevails up to the position of $z/H = 2.0$, because the main-channel vortex is too weax to influence the free-surface vortex. This feature is the same as in the rectangular open channel whose aspect ratio is greater than 5. In the case of S-3, the main-channel vortex expands in the

spanwise direction, and it forms a rather flat vortex in the region of $y/H > 0.5$. The downflow toward the corner of the main channel becomes noticeable below this main-channel vortex. This fact suggests strongly that the structure of secondary currents in the main channel becomes nearly equal to that in the narrow rectangular open channel, as the flood-plain region decreases. On the other hand, as the flood-plain region increases, the main-channel vortex beside the flood plain is stronger than the free-surface vortex near the side wall, as clearly seen in Fig. 15. As a result of the expansion of the mainchannel vortex in the spanwise direction, the free-surface vortex is reduced in both the size and strength. The position at which the downflow occurs moves toward the side wall of the main channel, i.e. $z/H = 1.25$ in the case of S-3, while this position in the case of S-2 is about $z/H = 1.6$, as seen in Fig. 6.

Fig. 15 (c) shows the vector description of the secondary currents in the case of R-1 which has the same value of h/H as case of S-2, but has a rough wall on the flood plain. In the case of R-1, it should be noted that the structure of secondary currents almost the same as that in the case of S-2 shown in Fig. 6. This means that there is only a slight effect of the roughness on the secondary currents, within the range of the present experiments. Tominaga et al. (1989) found that the roughness did not change the essential structure of secondary currents near the side wall of a rectangular open channel although it changed the size of longitudinal vortices. Naot(1984) indicated in a numerical calculation using an algebraic stress model that the effect of the roughness on secondary currents of a rectangular open channel appeared only in the near-wall region. From these facts, the effects of the wall roughness are not so predominant as those of the channel geometry, i.e. the ratio h/H of the flow depth of the flood -plain to the total flow depth.

4. 2 Primary Mean Velocity

Fig. 16 (a) and (b) show the isovels of the primary mean velocity in the cases of S-1 and S-3. The isovels near the junction in the case of S-1 bulge upward over a wide region. In spite of a large flow depth of the flood plain, the deceleration due to the low-momentum transport from the junction edge extends to the free surface. The curvature of the bulges are rather smaller than the case of S-2. The primary mean-velocity structure in the region $z/H < 1.75$ is almost the same as that of the rectangular open channel, which has been obtained by Nezu & Rodi(1985) and Tominaga et al. (1989). It should be noted that the isovel lines for Case S-3 do not bulge any longer from the junction toward the free surface, but they bulge rather toward the side walls of main channel in the same

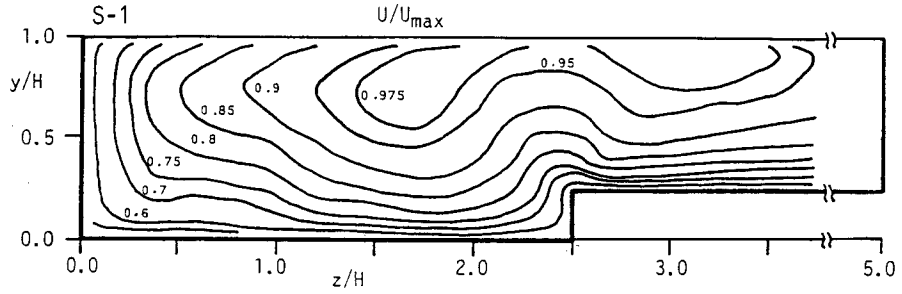

(a) Case S-1 (h/H=0.75)

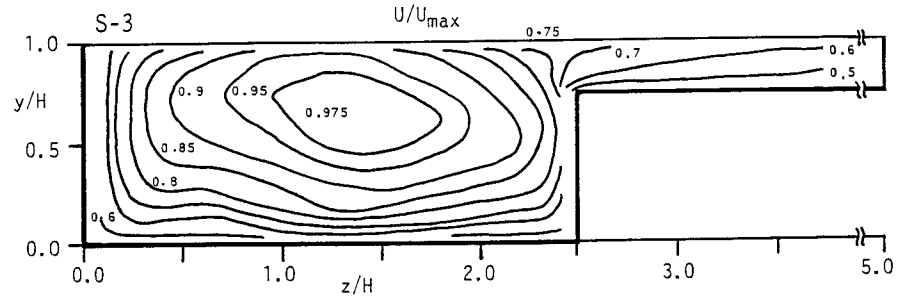

(b) Case S-3 (h/H=0.25)

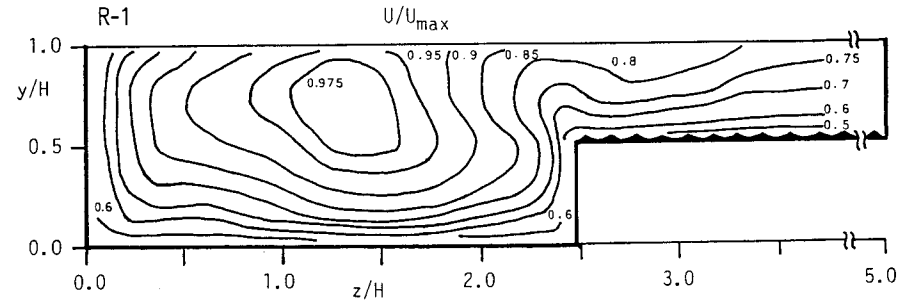

(c) Case R-1 (h/H=0.5 and rough on the flood plain)

Fig. 16 Isovels of Primary Mean Velocity U in Various Cases

manner as the rectangular open-channels. Of particular significance is that the maximum velocity appears considerably below the free surface. This velocity-dip phenomenon becomes more remarkable as the value of *h/H* decreases.

Fig. 16 (c) shows the isovels of the primary mean velocity in the case of R-1. Comparing the rough condition of Fig. 16 (c) with the smooth condition of Fig. 8,

the velocity on the rough flood plain becomes smaller than that on the smooth flood plain due to the retarding effect of the wall roughness. Although the isovels bulge along the inclined upflow in the same manner as the case of S-2, the bulge of isovels toward the bed of the flood plain becomes weak. The structure of U/U_{max} in the region $z/H \leqq 1.5$ is almost the same as the case of S-2, whereas U/U_{max} in the region $1.5 \leqq z/H \leqq 2.5$ is slightly more decelerated than U/U_{max} in the case of S-2.

4. 3 Distributions of Bed Shear Stress

The bed shear stress is important in hydraulic and river engineerings, because it governs sediment transport. The distributions of bed shear stress in each case are compared in order to examine the effect of the channel geometry and the wall roughness. The friction velocity U_* could be evaluated reasonably from the log-law distribution, as mentioned previously. The bed shear stress τ was then calculated from $\tau=\rho U_*^2$, where ρ is the water density. The discrepancy between the value of the bed shear stress $\bar{\tau}$ averaged in the spanwise direction and the overall value of ρgRI (where, I is the energy gradient and R is the hydraulic radius) was within only 6 % in all cases.

Fig. 17 shows the distributions of the bed shear stress on both mainchannel and the flood-plain beds, which are normalized by the averaged shear stress $\bar{\tau}$. Noticeable features in the distribution of the bed shear stress $\tau/\bar{\tau}$ are recognized on the flood-plain bed in compound open-channel flows. The bed shear stress on the flood plain increases rapidly as the junction edge is approached. This increase of the bed shear stress on the flood plain becomes greater with a decrease of h/H. This phenomenon was also observed by Rajaratnam & Ahmadi (1981). They pointed out that such an excess of the bed shear stress on the flood plain indicated the amount of spanwise momentum transport from the main channel.

The distribution of the bed shear stress shows an inflection point due to the effect of the bottom vortex at the position $z/b \simeq 0.2$ near the sidewall of the main channel, as pointed out by Tominaga et al. (1989) in the rectangular open-channel flows. However, such an inflection point does not apper near the junction side wall. The position at which the value of τ on the main channel attains a peak moves from the junction toward the side wall of the main channel, as the value of h/H decreases. Although the value of τ on the flood plain becomes large due to the wall roughness in the case of R-1, the distribution of τ over the main channel bed is nearly equal to that of the smooth bed in S-2. This fact implies that the spanwise interaction between the main channel

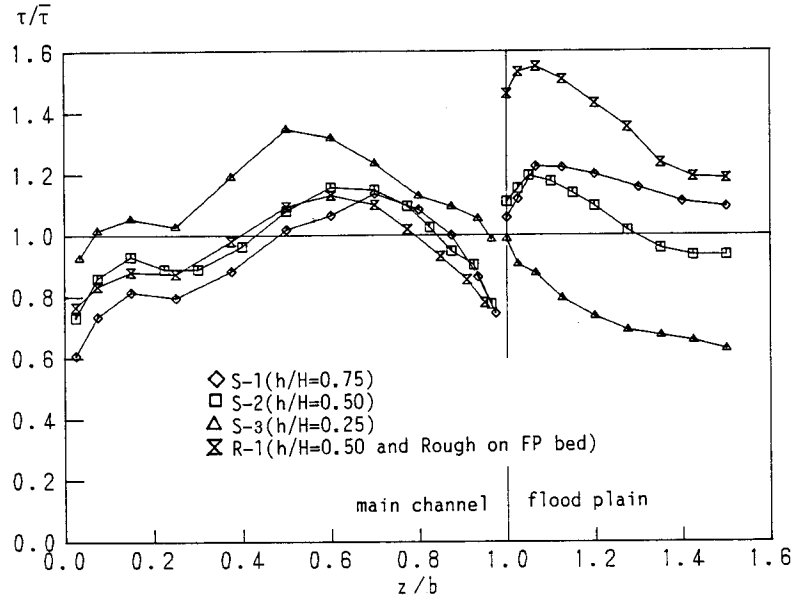

Fig. 17 Distributions of Bed Shear Stress

and flood plain flows is almost the same in the smooth and rough compound open-channel flows.

5. Interaction of Main Channel and Flood Plain Flows

The existence of secondary currents in compound open-channeld flows was verified from the present experiments, and influenced the threedimensional structures of the mean velocity and turbulence. Therefore, the contribution of the secondary currents to the momentum transport is investigated on the basis of the Reynolds equation. The equation of the streamwise component in a fully-developed turbulent open-channel flow is given, as follows:

$$\underbrace{V\frac{\partial U}{\partial y}}_{A_v}+\underbrace{W\frac{\partial U}{\partial z}}_{A_w}=\underbrace{gI_e+\frac{\partial(-\overline{uv})}{\partial y}}_{R_{uv}}+\underbrace{\frac{\partial(-\overline{uw})}{\partial z}}_{R_{uw}}+\underbrace{\nu\left(\frac{\partial^2 U}{\partial y^2}+\frac{\partial^2 U}{\partial z^2}\right)}_{VIS} \tag{14}$$

in which I_e is the energy gradient and g is the gravitational acceleration. All of the terms in the Eq.(14) could be calculated using the present experimental values.

The isolines of the advection terms A_w due to secondary currents, and the

isolines of the vertical Reynolds stress term R_{uv} containing the gravity term are shown in Fig. 18, together with isolines of the spanwise Reynolds stress term R_{uw}. The term of VIS means the viscosity, and it can be neglected except for very near the wall. If there exist no secondary currents, i.e. $V=W=0$, Eq.(14) reduces to $R_{uv}=0$. That is to say, the vertical Reynolds stress $-\overline{uv}$, of course, obeys the linear distribution in two-dimensional flows without any secondary currents. These values are normalized by $\overline{U}_*^2/H$, and the hatching area indicates a region of negative values.

The absolute values in Eq.(14) become very large near the junction edge, as clearly seen in Figd 18. The values of A_v and R_{uw} indicate large positive values in the region just above the junction edge. The magnitude of both terms in this region is almost the same as each other. In the flood-plain region adjacent to this positive region, A_v and R_{uw} indicate negative values which are almost the same order of magnitude. Consequently, the values of A_v balance well with R_{uw} in the junction region abouve the floodplain level. However, R_{uw} indicates a negative value near the side wall at the junction, whereas A_v indicates a positive value. This unbalance is compensated by the spanwise advection term A_w and the vertical Reynolds stress term R_{uv}. On the other hand, the values of A_w and R_{uv} indicate large positive values in the main-channel region just below the inclined secondary upflow. The values of A_w and R_{uv} in this region are almost the same order of magnitude. It is noted that the positive isolines of A_v and R_{uw} bulge toward the vertical direction from the junction edge, whereas those of A_w and R_{uv} bulge toward the inclined upflow direction from the junction edge. Shiono & Knight(1989) also investigated the mechanism of the momentum transport in a compound open channel with a relatively low flood-plain depth. When h/H is small, the importance of A_v is considered to be relatively small.

It is very important in compound open channel flows to evaluate the spanwise momentum transport from the main channel to the flood plain. In order to examine the effect of secondary currents on the spanwise momentum transport, Eq.(14) is integrated over the flow depth. The depth-averaged momentum equation in a fully-developed turbulent open-channel flow is then obtained from Eq.(14), as follows:

$$\frac{\tau(z)}{\rho}=gh'I+\frac{d}{dz}(h'\cdot T)-\frac{d}{dz}(h'\cdot J) \tag{15}$$

$$T=\frac{1}{h'}\int_0^{h'}(-\overline{uw})dy,\ J=\frac{1}{h'}\int_0^{h'}(UW)dy \tag{16}$$

in which h' is the flow depth; $h'=h$ in the flood plain, while $h'=H$ in the main

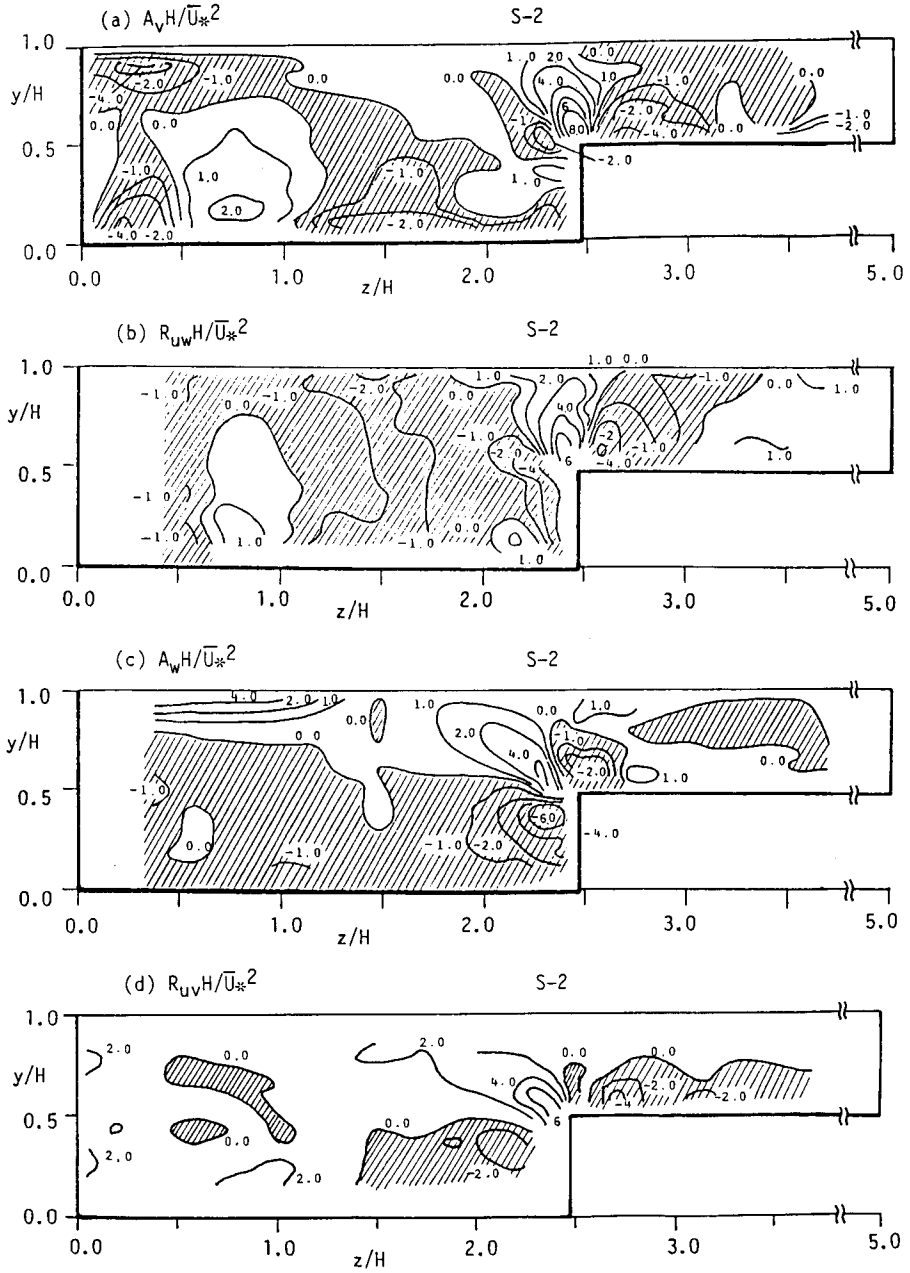

Fig. 18 Structures of Each Term in Reynolds Equation

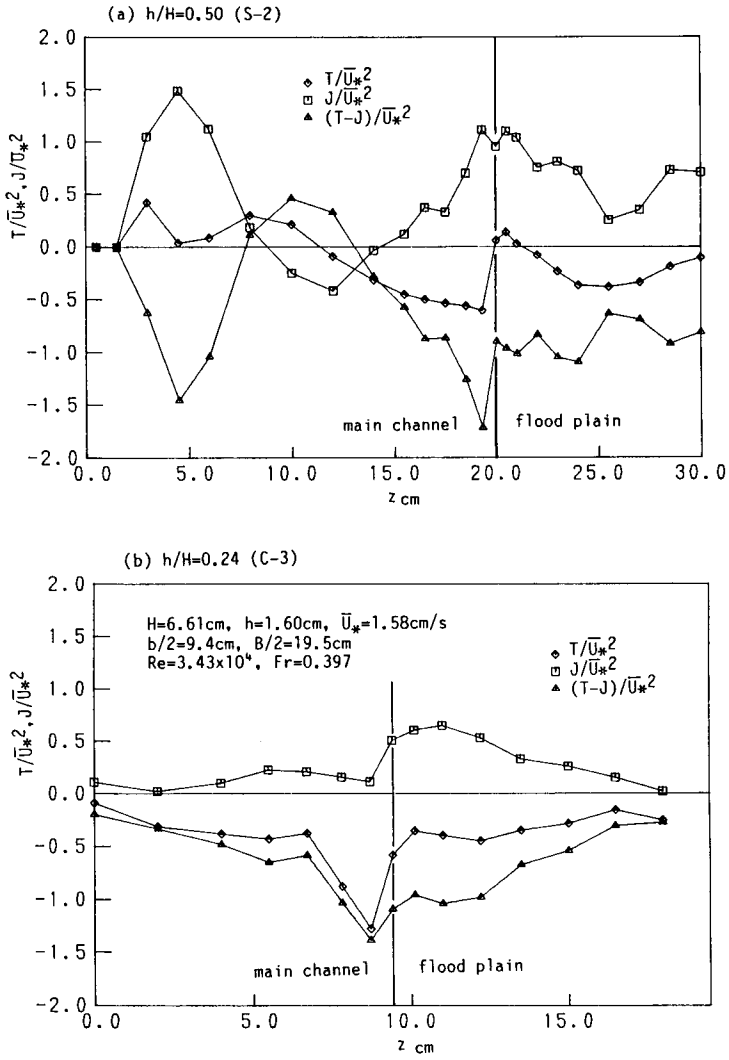

Fig. 19 Spanwise Distribution of Apparent Shear Stress

channel. $\tau(z)$ is the bed shear stress which corresponds to the total shear stress $(-\overline{uv}+\nu\partial U/\partial y)$ at $y=0$. T is the shear stress due to the spanwise Reynolds stress and J is the spanwise advection due to the secondary velocity W. The value of $(T-J)$ indicates an apparent shear stress acting on a $x-y$ plane at the position z, and it represents the magnitude of the spanwise momentum transport.

Fig. 19 (a) and (b) show the spanwise distribution of the apparent shear stress $(T-J)$, together with the advection term J and the Reynolds stress term T

which were evaluated from the experimental values. The experimental data plotted in Fig. 19(b) were obtained from Tominaga et al. (1989), who have measured with hot-film anemometers in a symmetrical compound openchannel flow. The value of J attains a positive peak at the junction edge, irrespective of $h/H=0.5$ and 0.24. These peak values of J are nearly equal to U_*^2 and $0.6\,U_*^2$, respectively. On the other hand, the distributions of T are quite different from each other at $h/H=0.5$ and 0.24. The value of T attains a large negative peak in the main-channel region very near the junction edge. On the other hand, the value of T attains a small positive peak in the flood plain very near the junction edge in the case of $h/H=0.5$. Generally speaking, the absolute values of the advection term J are greater than the values of the Reynolds stress term T near the junction in the case of $h/H=0.5$. On the other hand, in the case of $h/H=0.24$, the former is smaller than the latter in the main channel, but the former is greater than the latter in the flood plain. Consequently, the total apparent shear stress attains a negative peak in the main-channel region very near the junction edge, irrespective of $h/H=0.5$ and 0.24.

It is important to estimate the magnitude of the momentum transport due to the secondary currents between the main channel and the flood plain in compound channel flows. The distribution of W is assumed by a linear distribution;

$$W=W_{max}(1-2y/h) \tag{17}$$

in which W_{max} is the maximum value of W. Since the distribution of U is given by Eq.(13), J can be calculated from Eq.(16), as follows;

$$J=\frac{1}{h}\int_o^h W_{max}(2y/h-1)\left(\frac{U_*}{\kappa}ln\frac{U_*y}{\nu}+AU_*\right)dy=1.25W_{max}U_* \tag{18}$$

The experimental values of W_{max} are nearly equal to $0.7\,\overline{U}_*$. Therecore, the convection term J is estimated from Eq.(18) to be nearly equal to U_*^2. This calculated value coincides well with the observed value near the junction, as seen in Fig. 19(a).

Rajaratnum & Ahmadi(1981) indicated that the apparent shear stress became extremely large, as h/H decreased. For example, according to their experiments, the value of $(T-J)$ became equal to about $10\,\overline{U}_*^2$ at $h/H=0.1$. In such a case, the Reynolds stress term T is expected to be dominant, as compared with the advection term J.

6. Conclusions

In the present study, a 3-D turbulent structure of compound open channel flows has been investigated experimentally. All three components of the mean velocity and the five components of the Reynolds stress could be obtained from the present 3-D measurement system using a fiber optic laser Doppler anemometer (FLDA) in which the optical probe was set up beside the side wall of the channel and above the free surface. The secondary velocities obtained from the present FLDA system sufficiently satisfied the equation of continuity, although the magnitude of the secondary velocity was within only a few percent of the main flow velocity. Therefore, it was concluded that the present experimental data obtained from the FLDA were very accurate.

Of particular significance is that the strong inclined secondary currents are generated from the junction edge toward the free surface in compound open-channel flows. When the flow depth of the flood plain is equal to half the flow depth of the main channel, the secondary currents become strongest. The maximum magnitude of this inclined secondary upflow was about 4% of the maximum main-flow velocity U_{max} in the case of $h/H = 0.5$. A pair of longitudinal vortices are recognized on both sides of the inclined upflow. The vortex on the side of the flood plain is called the "flood-plain vortex", whereas the vortex on the side of the main channel is called the "main-channel vortex".

The isovel lines of the primary mean velocity bulge upward in the vicinity of the junction edge along the inclined upflow. The structure of the primary mean velocity is affected by the momentum transport due to the secondary currents.

Three-dimensional structures of Reynolds stresses and turbulence intensities were revealed in compound channel flows. The value of $-\overline{uv}$ increased just above the junction edge, but it indicated a negative value below this region. The value of $-\overline{uw}$ attained positive and negative peaks alternately near the junction edge. The sign of $-\overline{uv}$ and $-\overline{uw}$ corresponded to the sign of $\partial U/\partial y$ and $\partial U/\partial z$, respectively. These facts suggest that the eddy viscosity model is valid even in such a complex compound open-channel flow. All three components of the turbulence intensities increase in the vicinity of the junction edge. Of particular significance is that the isolines of v' are quite different from those of w'. The minimum values of u' and w' didn't appear on the free surface, but appeared below it in the main channel, like the velocity-dip phenomenon. On the other hand, the value of v' decreased monotonically as the free surface was

approached. One can understand from the equation of vorticity that such a strong anisotropy of turbulence near the junction and near the free surface generates the longitudinal vortices, i.e. the main-channel vortex and the flood-plain vortex.

When h/H is large, i.e. $h/H = 0.75$, the main-channel vortex wasn't recognized clearly, while the flood-plain vortex was strong enough to reach the free surface. On the other hand, when h/H is small, i.e. $h/H = 0.25$, the main-channel vortex expands in the spanwise direction. The position at which a downflow occurred moved toward the side wall of the main channel, as h/H decreased. When the flood-plain bed was rough, the structure of the secondary currents was almost the same as that for the smooth bed. This means that the effect of the channel geometry, that is, the ratio of the flood-plain depth to the main-channel depth, is predominant over the effect of the wall roughness.

The present study found that the interaction between the main-channel and flood-plain flows was very important, because the contribution of secondary currents on the momentum transport is very large near the junction. The data base of the present experimental values is also very valuable to examine the validity of numerical calculations for three-dimensional compound open-channel flows, including the effect of the free surface.

Acknowledgment

This study was conducted under domestic collaboration between Kyoto University in western Japan and Gunma University in eastern Japan. The authors are thankful to Prof. H. Nakagawa at Kyoto University, and Prof. K. Ezaki and Prof. S. Kobatake at Gunma University.

References

Arnold, U., J. Stein and G. Rouve(1989) : Sophisticated Measurement Techniques for Experimental Investigation of Compound Open Channel Flow, Computational Modelling and Experimental Methods in Hydraulics, Elsevier, pp. 11 - 21.

Alavian, V. and V. H. Chu(1985) : Turbulent Exchange Flow in Shallow Compound Channel, Proc. of 210. IAHR Cong. Melbourne, pp. 447 - 451.

Bradshaw, P. (1987) : Turbulent Secondary Flows, Ann. Rev. Fluid Mech., vol. 19, pp. 53 - 74.

Brundrett, E. and W. D. Baines(1964) : The Production and Diffusion of Vorticity in Duct Flow, J. Fluid Mech., vol. 19, pp. 375 - 392.

Gessner, F. B. (1973:) : The Origin of Secondary Flow in Turbulent Flow along a Corner, J.

Fluid Mech., vol. 58, part 1, pp. 1 - 25.

Kawahara, Y. and N. Tamai(1989) : Numerical Calculation of Turbulent Flows in Compound Channels with an Algebraic Stress Turbulence Model, Proc. of 3 rd Symp. on Refined Flow Modelling and Turbulence Measurements, Tokyo, pp. 527 - 536.

Keller, R. J. and W. Rodi(1988): Prediction of Flow Characteristics in Main Channel/Flood Plain Flows, J. Hydraulic Research, vol. 26, pp. 425 - 441.

Knight, D. W. and J. D. Demetriou (1983): Flood Plain and Main Channel Flow Interaction, J. Hydraulic Eng., ASCE, vol. 109, pp. 1073 - 1092.

Knight, D. W. and Hamed, M. E. (1984), Boundary Shear in Symmetric Compound Channels, J. Hydraulic Eng., ASCE, vol. 110, pp. 1412 - 1430.

Krishnappan, B. G. and Y. L. Lau (1986): Tubulence Modelling of Flood Plain Flows, J. Hydraulic Engineering, vol. 112, No. 4, pp. 251 - 266.

Larsson, R. (1988): Numerical Simulation of Flow in Compound Channels, Proc. of 3 rd Symp. on Refined Flow Modelling and Turbulence Measurements, Tokyo, pp. 537 - 544.

Lai, C. J. and D. W. Knight (1988): Distribution of Streamwise Velocity and Boundary Shear Stress in Compound Ducts, Proc. of 3 rd Symp. on Refined Flow Modelling and Turbulence Measurements, Tokyo, pp. 527 - 536.

Mackee, P. M., E. M. Elsawy and E. J. Mckeogh (1985): A Study of the Hydraulic Characteristics of Open Channels with Flood-Plain, Proc. of 21 st IAHR Cong. Melbourne, pp. 361 - 366.

Melling, A. and J. H. Whitelaw (1976): Turbulent Flow in a Rectangular Duct, J. Fluid Mech., vol. 78, pp. 289 - 315.

Nalluri, C. and N. D. Judy (1985): Interaction Between Main Channel and Flood Plain Flow, Proc. of 21 st IAHR Cong. Melbourne, pp. 378 - 382.

Naot, D. (1984): Response of Channel Flow to Roughness Heterogeneity, J. Hydraulic Eng., vol. 110, No. 11, pp. 1568 - 1587.

Nezu, I. and W. Rodi (1985): Experimental Study on Secondary Currents in Open Channel Flow, Proc. of 21 st Congress of IAHR, Melbourne, vol. 2, pp. 19 - 23.

Nezu, I and W. Rodi (1986): Open-Channel Flow Measurements With a Laser Doppler Anemometer, J. Hydraulic Eng., ASCE, vol. 112, pp. 335 - 355.

Nezu, I., H. Nakagawa and W. Rodi (1989): Significant Difference of Secondary Currents in Closed Channels and Narrow Open Channels, Proc. of 23 rd Congress of IAHR, Ottawa, pp. A 125 - A 132.

Ogink, H. J. M. (1985): The Effective Coefficient in 2-D Depth-Averaged Flow Models, Proc. of 21 st IAHR Cong. Melbourne, pp. 475 - 479.

Pasche, E., G. Rouve and P. Evers (1985): Flow in Compound Channels with Extreme Flood -Plain Roughness, Proc. of 21 st IAHR Cong. Melbourne, pp. 384 - 389.

Prinos, P., R. Townsend and S. Tavoularis (1985): Structure of Turbulence in Compound Channel Flows, J. Hydraulic Eng., ASCE, vol. 111, pp. 1246 - 1261.

Prinos, P. (1989): Experimental and Numerical Modelling in Compound Open Channel and Duct Flows, Computational Modelling and Experimental Methods in Hydraulics, Elsevier, pp. 255 - 268.

Rajaratnam, N. and R. M. Ahmadi (1981): Hydraulics of Channels with Flood-Plains, J.

Hydraulic Research, vol. 19, pp. 43－60.

Shiono, K. and D. W. Knight (1989): Transverse and Vertical Reynolds Stress Measurements in a Shear layer Region of a Compound Channel, Proc. of 7 th Symp. on Turbulent Shear Flows, Stanford, 28－1.

Tominaga, A. and K. Ezaki (1988): Hydraulic Characteristics of Compound Channel Flow, Proc. of 6 th Congress of Asian and Pacific Division, IAHR, Kyoto, pp. 465－472.

Tominaga, A. and I. Nezu, K. Ezaki and H. Nakagawa (1989): Three-dimensional Turbulent Structure in Straight Open Channel Flows, J. Hydraulic Research, vol. 27, pp. 149－173.

Tominaga, A., I. Nezu and K. Ezaki (1989): Experimental Study on Secondary Currents in Compound Open Channel Flows, Proc. of 23 rd Congress of IAHR, Ottawa, pp. A 15－A 22.